Solid Freeform Fabrication 2018: Proceedings of the 29th Annual International Solid Freeform Fabrication Symposium – An Additive Manufacturing Conference
Reviewed Paper

EFFECT OF LASER ADDITIVE MANUFACTURING ON MICROSTRUCTURE EVOLUTION OF INOCULATED $Zr_{47.5}Cu_{45.5}Al_5Co_2$ BULK METALLIC GLASS MATRIX COMPOSITES

Muhammad Musaddique Ali RAFIQUE[1], Milan BRANDT[2], Mark EASTON[3], Dong QIU[4], Ivan COLE[5], Sabu JOHN[6]

[1,3,4]School of Engineering, RMIT University, City Campus, Carlton, VIC 3053, Australia

[2]Additive Manufacturing Precinct, RMIT University, City Campus, Carlton, VIC 3053, Australia

[5]ECP Director, Advanced Manufacturing and Fabrication, Enabling Capability Platform, RMIT University, City Campus, Melbourne, VIC 3000, Australia

[6]School of Engineering Cluster, Manufacturing, Materials and Mechatronics, RMIT University, Bundoora Campus, Bundoora VIC 3083, Australia

Abstract

Bulk metallic glass matrix composites are advocated to be material of future owing to their superior strength, hardness and elastic strain limit. However, they possess poor toughness which makes them unusable in any structural engineering application. Inoculation has been used as an effective means to overcome this problem. $Zr_{47.5}Cu_{45.5}Al_5Co_2$ bulk metallic glass matrix composites (BMGMC) inoculated with ZrC have shown considerable refinement in microstructure owing to heterogeneous nucleation. Efforts have also been made to exploit modern laser-based metal additive manufacturing to fabricate BMGMC parts in one step. However, the effect of laser treatment on inoculated material is unknown. In this study, an effort has been made to apply laser based additive manufacturing on untreated and inoculated BMGMC samples. It is observed that laser treatment not only refined the microstructure but resulted in change of size, morphology and dispersion of CuZr B2 phase in base metal, heat affected zone and fusion zone. This effect is documented with back scattered electron imaging. This provides a basis for further research to quantify this phenomenon and full-scale part development.

Keywords: Additive, bulk metallic glass, composites, inoculation, phase

Corresponding author: Muhammad Musaddique Ali RAFIQUE (ali.rafique@hotmail.com, s3469212@student.rmit.edu.au)

Introduction

Over time, there has always been a quest for hard, strong and tough material [1, 2] which can effectively withstand the loads encountered in practical extreme engineering problems. Various efforts have been made to achieve this [3, 4] and many new materials were developed. Although they were discovered in 1950s [5], very recently, bulk metallic glasses [6-10] have emerged as potential candidates to solve this problem [11]. They possess high hardness [12, 13] and strength due to parent glassy structure but have poor ductility, hence poor toughness and exhibit catastrophic failure under the action of external load [14-16]. This problem limits their application. Efforts have been made to overcome this problem by introducing crystallinity in the glassy matrix. This may be achieved by various means including; external [17-19] introduction of reinforcing particles (*ex situ*) or internal (*in-situ*) [20-26] precipitating of same during processing (solidification [27-29], devitrification [30-33], powder metallurgy [34], foaming [35] or solid-state processing). However, this quest is still far from exhausted. Narrowing down the approach, *In-situ* introduction of precipitates during solidification have proved out to be the best mechanism to tackle this problem and newer methods have been introduced to achieve this mostly by control of melt composition [36], chemistry, and adjustment of processing conditions [37, 38]. Successful introduction of precipitates to form a composite structure was reported for the first time by Prof. Johnson's group at Caltech in 2000 [39]. Since then many groups in the world have produced a multitude of composites using similar philosophy [21, 28, 40-56]. As for the technique, very recently, additive manufacturing has emerged as new innovative and competitive route for a quick, efficient and one step solution to produce near net shape complex parts [57-61]. Components from nearly all types of metals and alloys can be produced by this technique (laser [58-60, 62, 63] or electron beam [64, 65] based) as the temperature obtained is a function of laser power and can be flexibly controlled over a wide range. Seeing its potential, need and interest has also sparked in the use of this technique for microstructure control [54, 66-68], manipulation [69, 70] and manufacturing of parts by bulk metallic glasses and their composites [55, 67, 71-73]. Both simulation [55, 63, 65, 74-80] and experimental [64, 67, 68, 81, 82] methodologies have been rigorously applied to study, determine and ascertain the effect of various material and process parameters on final part quality and its properties. Different AM variants such as laser surface remelting [38, 54, 66-69, 83-89], 3D printing [90-94] LENS [95], welding [96-98], pulsing [99, 100], shock peening [101], and laser solid forming [66, 69, 99-103] have been successfully applied to fabricate parts of various types, size, nature and geometries. Recently, an established grain refinement technique – inoculation [3, 104, 105] has been applied to Zr based bulk metallic glass matrix composites and found to successfully improve properties of as cast composites [28, 106]. However, the effect of the incidence of a high energy laser with varying scan speeds on these inoculated composites is not known – an important parameter for full scale part development. Gaps exist in the literature and reported research in how these versatile materials whose grain structure has been improved by inoculation will behave under intense source of heat energy (laser)? What will be the effect on type, size, distribution and morphology of phases as well as size, dimensions and geometries of associated melt pools, heat affected zones and unaffected base material? The present study is aimed to bridge this gap. A systematic study is carried out in which bulk metallic glass matrix composites with different percentages of ZrC subjected to a laser source of constant size (spot size). The effect of laser power and scan speed are evaluated.

Experimental procedure

As cast bulk metallic glass matrix composites were produced using vacuum arc melting and suction casting button furnace. They were produced by mixing appropriate amounts of pure elements Zr, Cu, Al and Co with different percentages of ZrC inoculant such that a small button is produced which was placed in the hearth of furnace and melted with the help of an arc. The melted volume was placed on a small orifice and sucked through a chute into a copper mold beneath using negative pressure generated by a vacuum pump. The sucked volume adopted the shape of copper mold and generated a gradient of microstructure across its length due to the difference in cooling rate. Resulting cast parts were cut into different small pieces and subjected to laser additive manufacturing on Trumpf® laser additive manufacturing machine with different parameters. *Laser additive manufacturing:* Samples were placed in the enclosed chamber and machine was operated in a condition of over pressure of inert gas. Three tracks were produced on each of three samples. The first one was made with 500 W power, 0.61 mm spot size and 600 mm / minute~~s~~ scan speed, second one was made with 300 W power, 0.61 mm spot size and 600 mm / minute~~s~~ scan speed while third one was made with 300 W power, 0.61 mm spot size and 1500 mm / minute~~s~~ scan speed. In all three cases, the spot size was kept constant while the power and scan speed were varied to check their effect on final microstructure. An increase in laser power was assumed to exert more energy input, cause more turbulence in the melt pool, increase spatter [3], denudation zones [55, 76], evaporation and distort the surface structure with irregularities (shrinkage, segregation, lapping, cracks, porosity, pin and gas holes [3, 104]) produced during solidification [4, 105, 107, 108]. High laser power is also proposed to induce solid state transformations [109] in solidified melts. These defects are even more pronounced at varying scan speeds and produce range of melt pool geometries [64], shapes and morphologies with a multitude of solidification microstructures. After laser surface treatment, samples were prepared for metallographic examination. *Sample preparation:* For metallographic sample preparation, the laser treated half wedge and strip were further cut at 2/3rd of distance from tip so that the area containing composite structure and effect of laser on it were exposed. Test coupons of 35 mm length, 18 mm width and 2 mm thickness were mounted with the exposed surface facing downward in 25 grams Stycast epoxy resin with 25 grams Buehler conductive filler. Mounts were cured at room temperature for 8 hours. Once cured, they were placed in Thermolyne Type 48000 furnace at 50ºC for 2 hours to harden the final epoxy. Cured mounts were subsequently subjected to grinding and polishing. Grinding was performed using silicon carbide papers to 240 grit and the samples were polished using 9 µm, 3 µm and 1 µm Diamond Duo polishing solution. Final polishing was done by employing 0.04 µm colloidal silica solution for 5 minutes. *Scanning electron microscopy:* Back scattered electron microscopy of laser surface treated inoculated samples was performed on a JOEL 7001F FE-SEM equipped with thermally assisted Schottky type field emission gun at The University of New South Wales, Sydney, Australia. Microscope was operated at cathode voltage of 15 KV. Sample was placed in chamber at a vacuum of 10^{-6} mbar created by the diffusion pump connected to it. Secondary electron imaging was performed by a collection of electrons at wall mounted secondary electron (Everhart Thornley type) detector (not shown). Back scattered electron imaging was carried out by back scattered electron detector. These electrons carry information about compositional contrast and clearly identify areas where microstructure is 100%

glass, affected by heat (heat affected zone) and remain unaffected and unaltered (base metal). Working distance was maintained at 10.7 ± 0.1 mm.

Results and discussion

Electron microscopy in back scattered imaging mode was performed in all three zones (base metal, heat affected zone and fusion zone) for each and individual track of laser on all three (untreated, inoculated with 0.25% and 0.5% ZrC) samples.

$Zr_{47.5}Cu_{45.5}Al_5Co_2$ (inoculant = 0%) Track 1

This track was laid with following parameters; Power 500 W, Spot size 0.61 mm, Scan speed 600 mm / min**.** Three distinct regions may be identified in micrographs of cross section of sample taken at low magnification (Figure 1 (a)). These were labelled as A, B and C which may be attributed to fusion / melt zone, heat affected zone (HAZ) and untreated / base metal zone respectively. For this sample with given parameters, a very large, wide and deep fusion zone was formed. This is due to very high power of laser which caused localised concentration of energy resulting in incipient fusion. At the same power of laser complete melting and rapid solidification of CuZr B2 [20] occurred. This can be observed by the appearance of 100% glassy structure in region A (Figure 1(b)). Another very important characteristic of this zone was formation of spherulites. These were consistent with observations made in a previous study [54] and were in contradiction to nanocrystalline phases observed upon isothermal annealing [110, 111]. Due to the rapid heat extraction and dissipation, these non-equilibrium products were formed. The width of melt pool or fusion zone was approximately 600 μm at the surface while its depth was 300 μm. There was shrinkage of approximately 30 – 40 μm at the top in the middle. Corners or edges of the melt pool were also blurred or torn apart and showed signs of deterioration due to intense heat generated by highly localised source of heat (laser). As the point of observation moved away from region A, a region which was depicted by mixed or hazy areas was observed. This is zone where incomplete transformation occurred, and the structure tends to freeze or coexist as crystalline metastable phase and glassy matrix. This happened as insufficient time was given to allow for complete dissolution of solid to liquid and then from liquid back to solid. This was known as the heat affected zone (HAZ). As the name suggest, it was region which was affected by heat, but remained incompletely transformed. Some phases or features were transformed, while others remained untransformed. It appeared as a distinct region in this sample. The width of this region ranged from 120 – 140 μm. Finally, as the point of observation moved further deep into sample, the base metal or untreated sample was observed (Figure 1 (d)). This was characterised by observation of well-known and documented spheroidal CuZr B2 phase [20]. There were few small brittle Al_2Zr fcc [112] dendrites emerging from background of glassy liquid. Phases formed were indicated by light colour while glassy matrix appeared as dark background. Evidence of small porosity was also observed which appeared as areas of black colour indicating empty space.

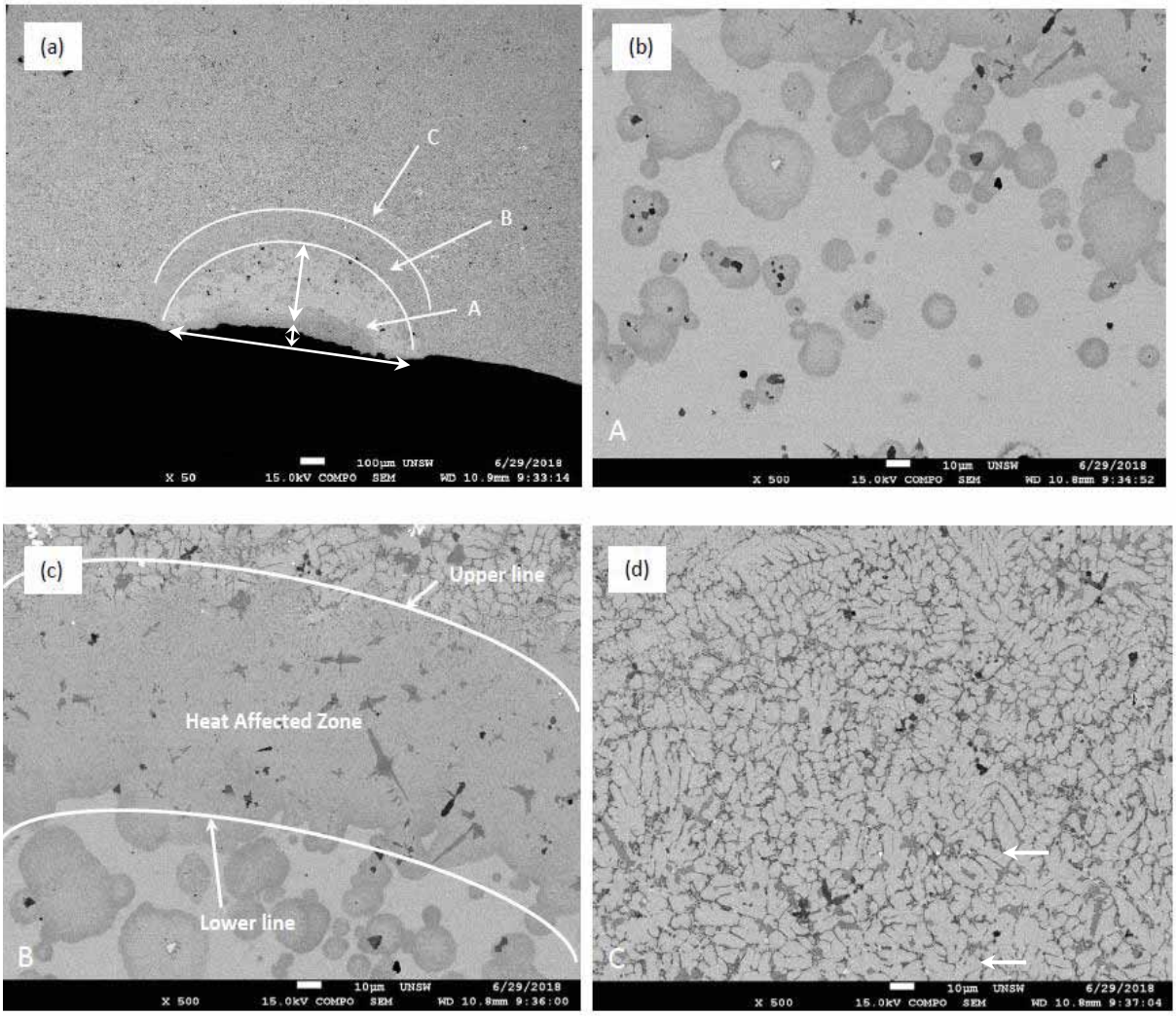

Figure 1 (a) – (d): $Zr_{47.5}Cu_{45.5}Al_5Co_2$ (0% inoculant) Track 1, (a) low magnification (x50) image of cross section of laser track, (b) Back scattered electron image of fusion zone / melt pool indicating formation of glass and spherulites avoiding nanocrystallites, (c) back scattered electron image of heat affected zone and (d) back scattered electron image of base metal indicating presence of different phases (CuZr B2 and small Al_2Zr fcc phase [112])

$Zr_{47.5}Cu_{45.5}Al_5Co_2$ (inoculant = 0%) Track 2

This track was produced with following parameters; Power 300 W, Spot size 0.61 mm, Scan speed 600 mm / min**.** Once again, three distinct regions may be identified in micrographs of cross section of sample taken at low magnification (x50) (Figure 2 (a)). Once again, these were labelled as A, B and C which were representation of fusion / melt zone, heat affected zone (HAZ) and untreated / base metal zone respectively. For this sample, with given parameters, a large, wide and deep fusion / melt zone was observed. This again was due to the high power of the laser which resulted in concentration of energy causing incipient fusion and formation of melt pool. As the spot size and scan speeds were kept constant while laser input power was reduced, it resulted in less deep melt pool. Also, there was less evidence of turbulence caused by reduced laser power. There was

some blurring or inconsistency at the top of melt pool but still, it was not as evident as was the case when laser power was 500 W. Some cracking was also observed at the edges of heat affected zone (HAZ). This was due to the difference in temperatures between the melt pool and base metal which caused thermal stresses. Another reason for this may be attributed to emergence of different coefficients of thermal expansion in metal solidified at melt pool (glass) and the composite structure of base metal. Another phenomenon of interest observed in this track was the emergence of small precipitates in the melt pool region (Figure 2(b)). These appeared in the form of small equiaxed grains. These may be an indication of incomplete fusion due to the low energy input. Another reason for this may be attributed to complete melting due to intense localised heating, freezing and then precipitation of large number of small equiaxed grains from the glass (recrystallisation / devitrification) because of heating below glass transition temperature (T_g). There was no evidence of change in morphology. Another possibility which may be considered was complete fusion and then CuZr B2 spheroidal phase precipitation from the rapidly solidifying melt. Their size was small as rate of heat extraction from the very small area was very fast which resulted in nucleation of large numbers of small grains because of suppressed kinetics. As the point of observation moved away from melt pool / fusion zone, a profound heat affected zone (HAZ) was observed in the form of boundary / interface between melt pool and base metal. This region

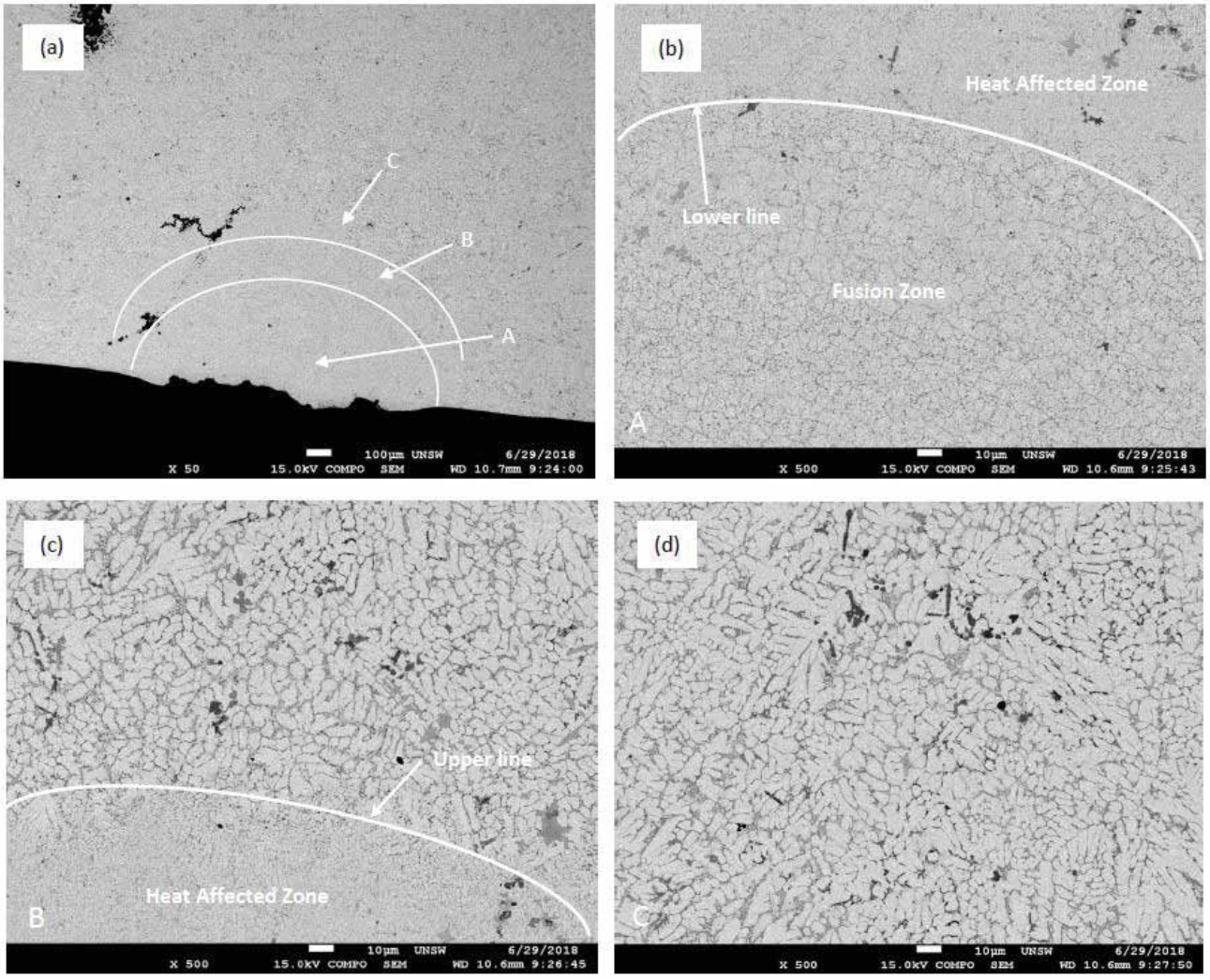

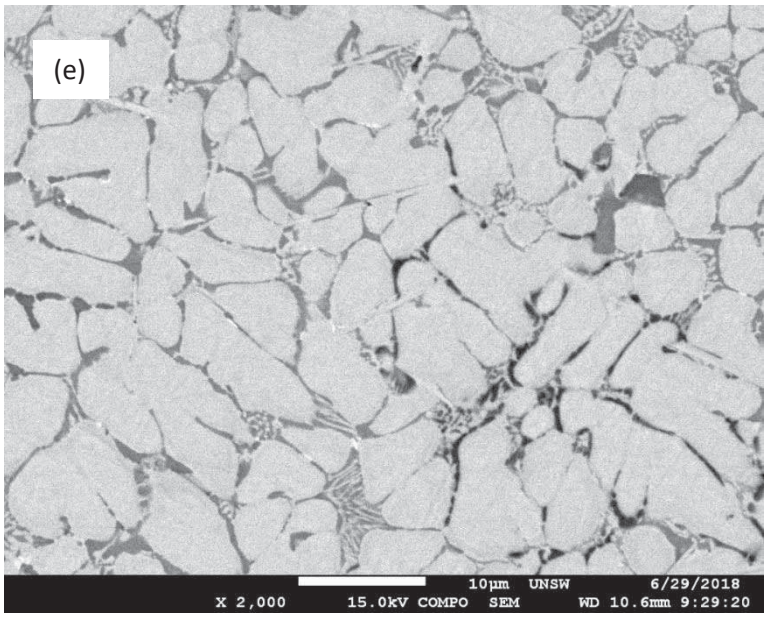

Figure 2 (a) – (e): $Zr_{47.5}Cu_{45.5}Al_5Co_2$ (0% inoculant) Track 2: (a) Low magnification (x50) back scattered electron image of cross section of laser track. (b) Melt pool and lower region of heat affected zone (x500), (c) Upper region of heat affected zone and its interface with base metal (d) Back scattered electron image of base metal indicating presence of CuZr B2 and small Al_2Zr fcc phase [112], (e) Base metal at higher magnification (x2500) indicating presence of glassy matrix (dark grey areas) and ductile precipitates (light areas).

was characterised by emergence of crystalline phases and a glassy matrix. However, as the laser power was low, its effect was not as profound as was when power was 500 W. Small cracks were also observed at the edges of the HAZ with base meal. The size of this region was around 120 – 140 µm. Once again, the reason for the cracking may be attributed to difference of temperature or coefficient of thermal expansion between different phases of material. Regular spheroidal shape CuZr B2 [20] precipitates were observed along with tree / flower like small brittle Al_2Zr fcc phase [112] as the point of observation moved further deep into sample towards base metal zone.

$Zr_{47.5}Cu_{45.5}Al_5Co_2$ (inoculant = 0%) Track 3

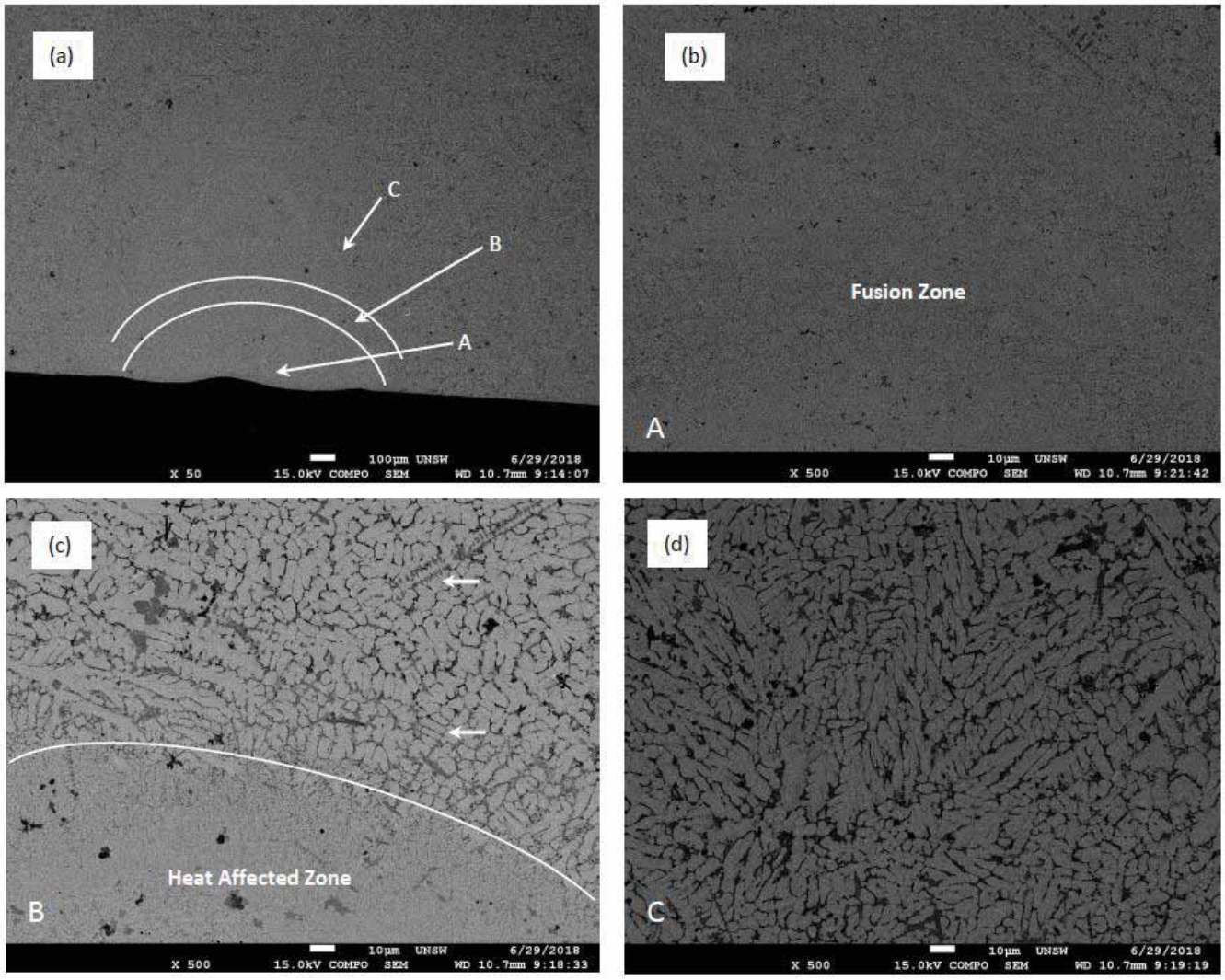

Figure 3 (a) – (d): $Zr_{47.5}Cu_{45.5}Al_5Co_2$ (0% inoculant) Track 3: Power 300 W, Spot size 0.61 mm, Scan speed 1500 mm / min, (a) Low magnification (x50) back scattered electron micrograph of cross section of laser track (b) Melt pool / fusion zone and lower region of heat affected zone (HAZ) at higher magnification indicating complete melting, solidification and 100% glassy structure, (c) Upper region of heat affected zone and its interface with base metal (d) Back scattered electron image of base metal indicating presence of CuZr B2 and small Al_2Zr fcc phase [112]. Different morphologies of phases can be observed as light areas originating from back ground of glassy matrix (dark areas).

This track was laid out with following parameters; Power 300 W, Spot size 0.61 mm, Scan speed 1500 mm / min. As the power and spot size were kept constant while scan speed was increased, it resulted in shallower and narrower melt pool or fusion zone as laser tends to move quickly in a given time over an area causing less abrupt action. Consequently, less volume was melted, and

only surface effects were observed. There was almost no turbulence and no pronounced effect of shrinkage was observed. Absence of turbulence also promoted homogenisation and fully glassy structure was formed without shrinkage, segregation and appearance of defects caused by movement of melt in confined volume, its interaction with environment (gases and air) and its entrapment. Size of melt pool was approximately 600 µm wide and 350 µm deep. There was small localised depression in the middle of pool which indicated localised shrinkage. As very less volume was melted and the interaction of energy with matter was extremely brief, size of heat affected zone was subsequently decreased and it spaned to a maximum width of 100 µm. Considerable decrease in size of heat affected zone (HAZ) indicated effectiveness and suitability of process to develop layer by layer (LBL) patterns as the need of removal of excess unwanted hard material was minimised. Grains in base metal region were mostly uniformly spaced. CuZr B2 tends to retain its near spheroidal morphology but was observed in sparse locations. Most of microstructure was filled with three dimensional small brittle Al_2Zr fcc phase [112] appearing in the form of randomly but uniformly distributed dendrites whose size ranged from 10 µm to 25 µm.

$Zr_{47.5}Cu_{45.5}Al_5Co_2$ (inoculant = 0.25%) Track 1

Track produced by incidence of laser on inoculated material surface, subsequent analysis of zones developed, and microstructure evolved in these were explained in figure 4 (a) - (d). These represent areas where laser energy produced different features on surface of inoculated material. These materials were characterised by presence of certain amount of ZrC inoculant. This imparted grain refinement to material and decreased the size of features (primarily CuZr B2) which can be easily observed in back scatter electron images of base metal (Figure 4 (d)). However, effect of laser generated different regions which will be explained in detail below. Laser parameters on this sample were; Power 500 W, Spot size 0.61 mm, Scan speed 600 mm / min. Figure 4 (a) showed general form and shape of melt pool. It indicated that melt pool was deep and narrow. This was due to intense heat generated by high powered laser localised in a confined area. This was backed up with a small spot size and slow scan speed which helped in further confinement of heat in small area and increased the depth to which it could penetrate. Overall width of melt pool and its depth was high as compared to width and depth when material of same composition without inoculants was subjected to laser surface treatment. Width of melt pool ranged to maximum of 900 µm while its depth extended roughly to 850 µm. Structure of melt pool showed complete fusion, dissolution of all precipitates, homogenisation / mixing, rapid cooling and formation of 100% glassy structure. There was marked indication of cracking due to intense heat generated in a confined area and sharp temperature gradient which existed between fusion zone and neighbouring cold base metal. Cracking may have also been caused due to frictional forces generated during grinding as the material was hard at fusion zone as compared to surroundings and this must have exhibited resistance to absorb energy and cracked. This crack extended all throughout the volume of material starting from surface towards base metal. Soon after fusion zone, an area depicted by intense effect of heat was witnessed. This was identified as heat affected zone (HAZ). This was area which was marked by incomplete / partial transformation. Size of this heat affected zone was very pronounced and profound in this sample. It ranged to maximum of 200 µm wide to 200 µm deep / long. An important feature was observed in this sample. This was presence of small crystals in partial or incompletely transformed glassy matrix. Appearance of these crystals may also be attributed to

inoculation effect itself. As there were stable inoculants present in melt which provided potent sites for heterogeneous nucleation, this sample showed appearance of small crystals even in heat affected zone. Presence of small hairline cracks indicated development of air pockets in solidifying metal. These may have also been caused by shrinkage. Finally, as the point of observation moved away from HAZ towards base metal, microstructure consisting of small precipitates (mainly CuZr B2) emerging out of glassy matrix was observed. This microstructure was characterised by finely dispersed crystals which were present all throughout the matrix. Size of these precipitates / crystals was on average around 2 – 6 μm while their morphology was spheroidal. They were dispersed all throughout the volume of material. They became the source of increase in ductility and toughness of material. There were other small precipitates present in matrix as well bearing dendritic structure which were small brittle Al_2Zr fcc phase [112]. They were consistent with similar structure observed in first glass matrix composite produced by Prof. Johnson's group [39].

$Zr_{47.5}Cu_{45.5}Al_5Co_2$ (inoculant = 0.25%) Track 2

As the laser power was reduced while keeping spot size and scan speed constant, structures shown in figure 5 (a) – (e) appeared. These clearly showed the effect of decrease in laser power which generated less heat and thus caused melting of less amount of material. This in turn generated small melt pool whose size was maximum 800 μm wide and 450 μm deep. Decrease in penetration depth was an indication that low power of laser did not generated enough heat at a point to cause deep impression. However, 100% glassy structure was formed and observed in melt pool which was an evidence that amount of heat was enough to cause complete fusion followed by rapid solidification. An important feature shown and observed in this sample was presence of small region in which no melting has occurred. This was characterised by a dark colour spot (Figure 5 (b)). This may have been produced because of unmelted ZrC inoculant particle at the centre of growing grain. The grain itself had not grown and may have been frozen due to extremely high cooling rate in a confined volume at the corner of small melt pool. There are few dark spots at top right corner of micrograph which indicated presence of porosity or gas holes. Once again, these may have been caused by poor melt treatment, improper casting practice or improper sample preparation.

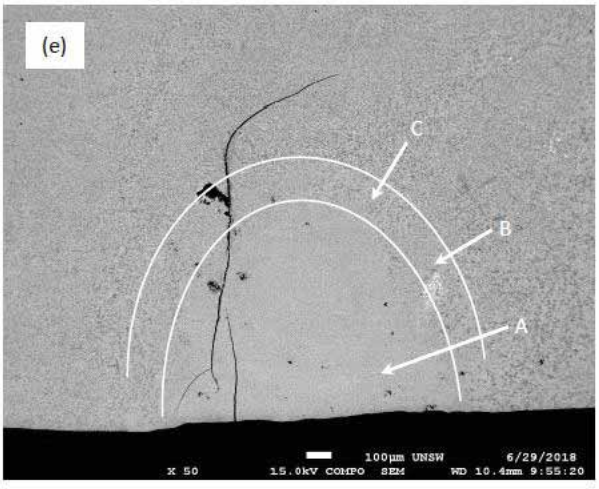

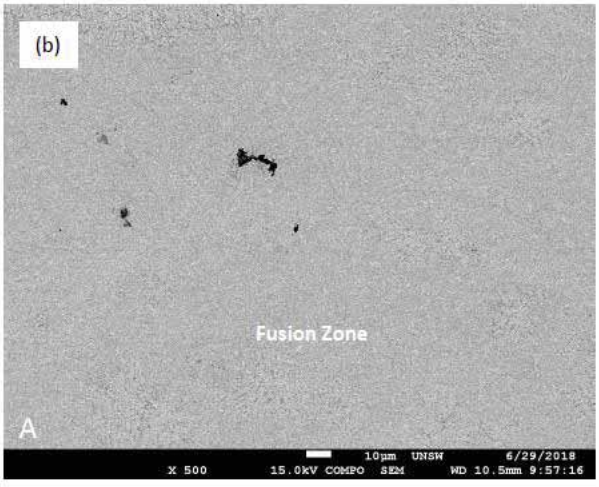

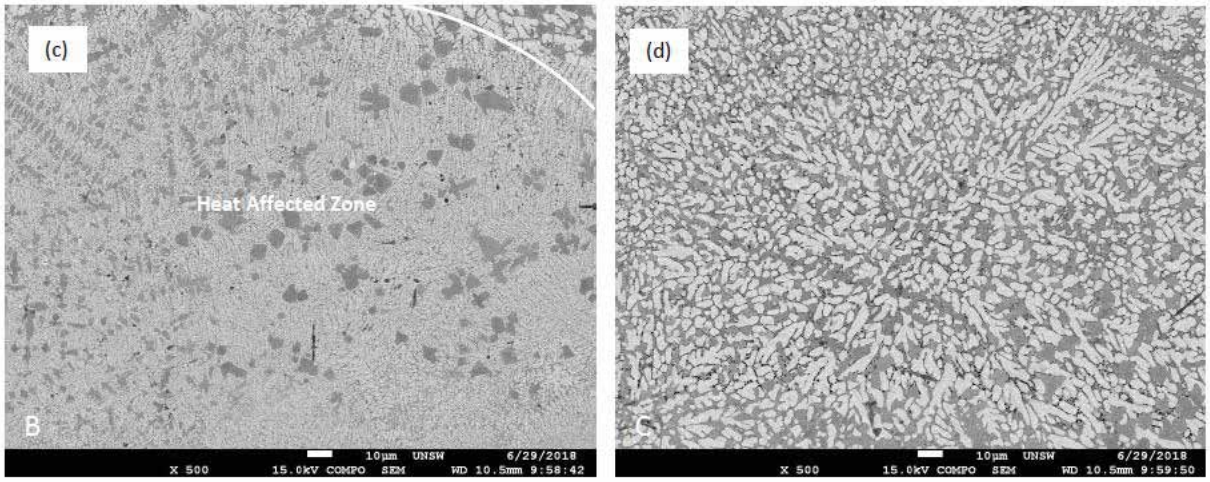

Figure 4 (a) – (d): $Zr_{47.5}Cu_{45.5}Al_5Co_2$ (0.25% inoculant) Track 1: Power 500 W, Spot size 0.61 mm, Scan speed 600 mm / min

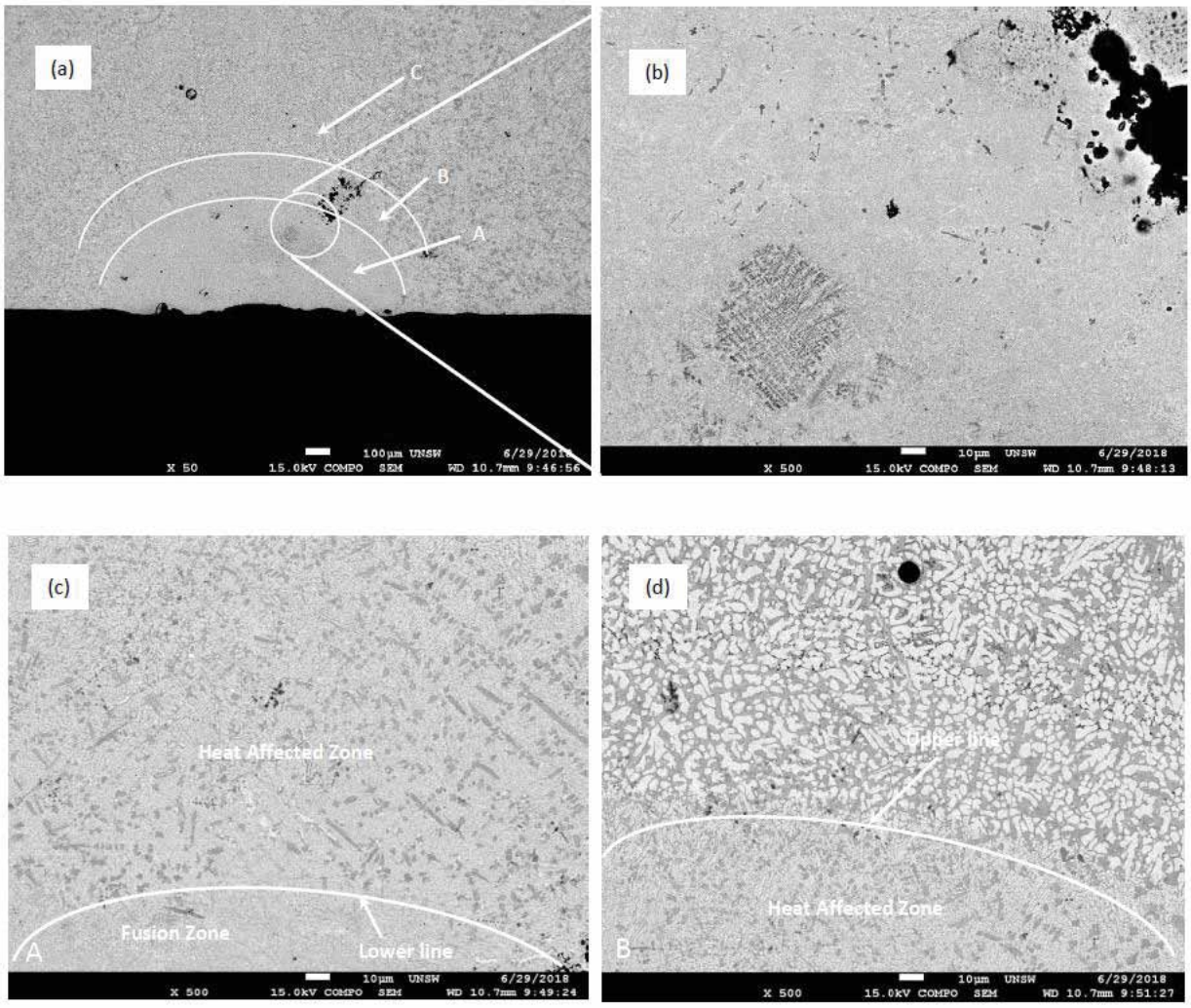

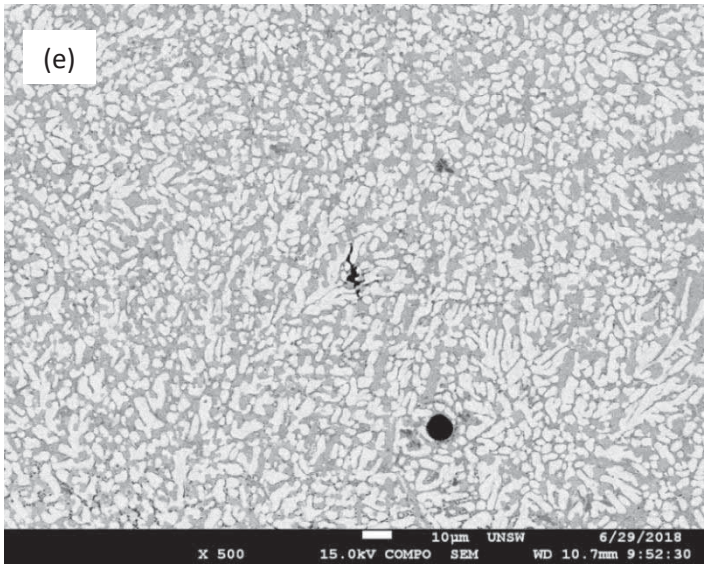

Figure 5 (a) – (e): $Zr_{47.5}Cu_{45.5}Al_5Co_2$ (0.25% inoculant) Track 2: Power 300 W, Spot size 0.61 mm, Scan speed 600 mm / min

As the point of observation moved away from melt pol, once again, an area bearing the effect of intense heat was observed, known as heat affected zone (HAZ) (Figure 5 (c)). Once again, due to prior inoculation it showed evidence of heterogeneous nucleation in which ductile crystalline particles tend to appear randomly in matrix despite of immense cooling rate observed there. Size of this zone was also very large spanning from approximately 200 µm wide to 250 µm deep. It was marked by a lower and an upper line. Mostly, equiaxed grains were observed in this region with a mix of glassy matrix. However, few small columnar grains were also observed at the interface of HAZ and base metal. They were formed because of difference of temperature between these two regions and heat transfer occurring as a result (Figure 5 (d)). Finally, as the point of observation moved to base metal, a microstructure independent of any impulse was witnessed. This was glassy matrix in which number of small CuZr B2 phases were uniformly distributed. Size of these crystalline phases was clearly decreased while their amount has increased. On average, their size was found to be around 1.8 – 2.5 µm. This was evidence of increase in toughness of these alloys which was observed in another study based on microhardness testing described by author elsewhere [113].

$Zr_{47.5}Cu_{45.5}Al_5Co_2$ (inoculant = 0.25%) Track 3

This track was laid out with following parameters; Power:300 W, Spot size: 0.61 µm, Scan speed: 1500 mm / minutes. Effect of this increased roaster / scan speed at power of 300W can easily be seen in development of small, shallow and narrow melt pool. Like previous sample, area exhibited by base metal consisted of small equiaxed precipitates originating from background of glassy matrix (Figure 6 (d)). These were mostly equiaxed in nature dispersed evenly all throughout the matrix. Melt / fusion zone on the other hand was manifested by complete fusion and formation of glass (Figure 6 (b)). There was no evidence of nucleation and growth or precipitation. Area known as heat affected zone (HAZ) which occurred in the middle of glassy matrix and base metal was shown in Figure 6 (c). Unlike previous heat affected zone (HAZ), the size of this area was reduced to width of almost 200 µm and depth of 180 µm. Primary reason of this was increased scan speed which decreased the time laser spent on metal surface thus created very short incipient melt pool

and associated heat affected zone. Morphology of crystallites in this region was again not quite well developed. However, presence of small Al_2Zr fcc phase [112] can easily be witnessed by appearance of dark areas (near spheroids or sharp needle like precipitates) emerging from the background of glassy matrix. This area was mostly marked by presence of metastable phase. There was almost no evidence of cracking, porosity, pin or gas holes and microstructure mostly showed uniformity.

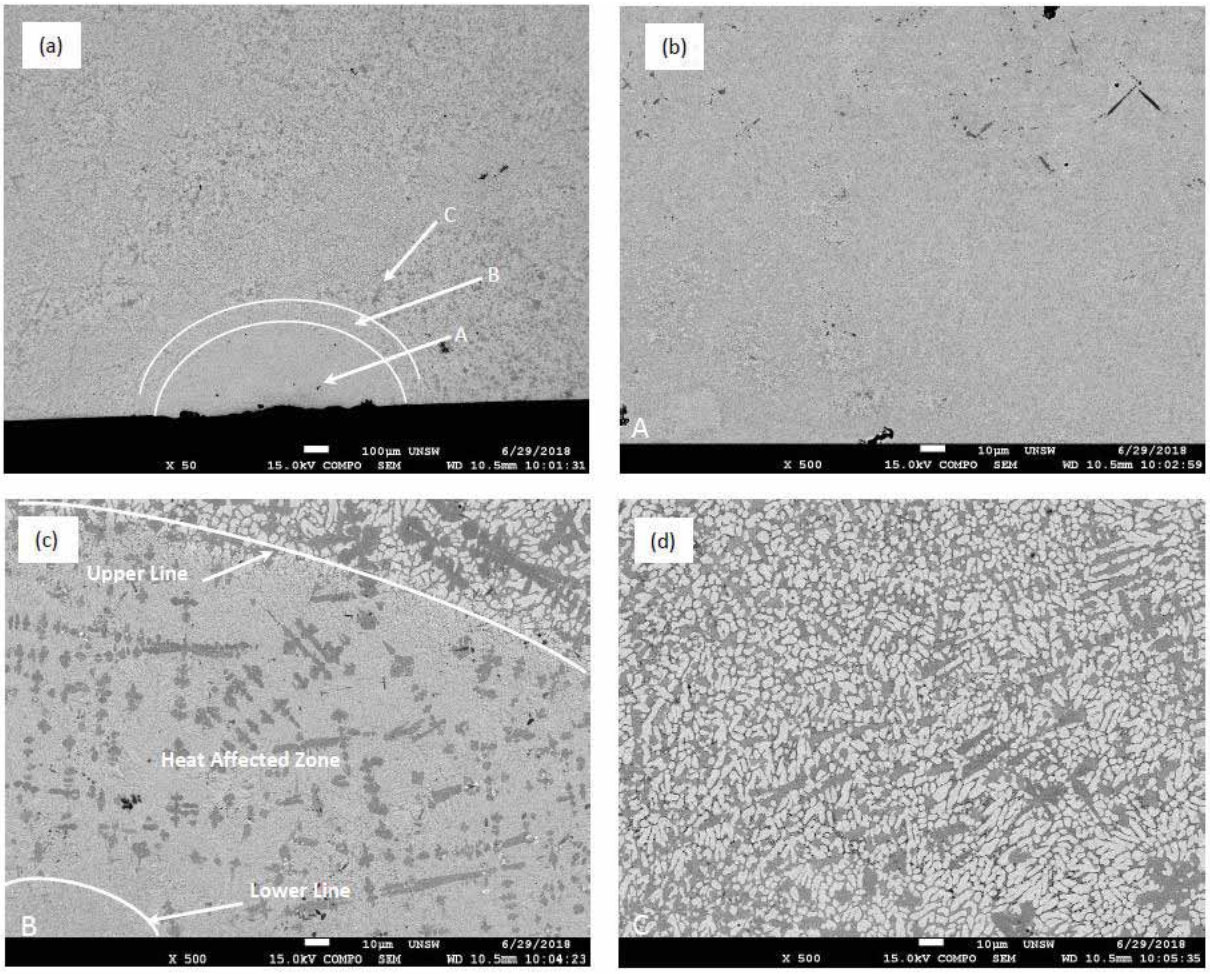

Figure 6 (a) – (d): $Zr_{47.5}Cu_{45.5}Al_5Co_2$ (0.25% inoculant) Track 3: Power 300 W, Spot size 0.61 mm, Scan speed 1500 mm / min

$Zr_{47.5}Cu_{45.5}Al_5Co_2$ (inoculant = 0.5%) Track 1

As the percentage of inoculant increased to 0.5%, a trend marked by increase in number density of phases developed was observed in as cast samples. This was optimistic indicator as a trend marked by increased toughness was expected (as reported previously [113]). However, change in type, size and morphology of same phases as affected by incident laser power was entirely different as will be explained in detail below. Figure 7 (a) showed low magnification (x50) image of melt pool when laser of 500 W stroked the sample with spot size of 0.61 mm and scan speed of 600 mm / minute. This area was marked by violent and turbulent movement of melt in confined space

when it got melted under the action of intense localised heat. There was a lot of surface roughness and sharp discontinuities on the surface. A marked depression was also observed on the surface indicating profound shrinkage. Total width / span of melt pool was calculated to be around 1000 µm at the surface while its depth was around 550 µm (highest point to bottom). The width of heat affected zone was small and may be calculated to be around 100 µm maximum. One reason which may be attributed to this was combination of speed and laser power. Also, it was anticipated that much of heat in this type of situation would be lost to atmosphere by surface exposure as melt pool was wide. When observed at higher magnification (x500), melt pool showed signs of complete melting followed by rapid solidification characterised by 100% monolithic glassy structure. No evidence of partial or complete crystallisation or recrystallisation was observed in melt pool and microstructure showed no sign of development of any feature (Figure 7 (b)). Soon after melt pool, an area marked by intense effect of heat on composite was observed known as heat affected zone (HAZ) (Figure 7(c)). This may be characterised into three regions. 1) Recrystallised region (light areas) (mostly these were recrystallised equiaxed CuZr B2 grains), 2) Al_2Zr fcc phase (dark grey areas) [112] and 3) Recrystallised columnar CuZr B2 grains. These are indicated by yellow arrow and found right at the interface / boundary of base metal and heat affected zone carrying equiaxed grains. Finally, when the point of observation moved further away from surface towards base metal, an area unaffected by the heat of laser was observed known as base metal. This was drastically characterised by presence of (a) small equiaxed CuZr B2 phase, glassy matrix (interdendritic dark areas) and Al_2Zr fcc phase (dark grey areas (profound dendritic structure)). There was also evidence of slight interdendritic shrinkage and micro porosity.

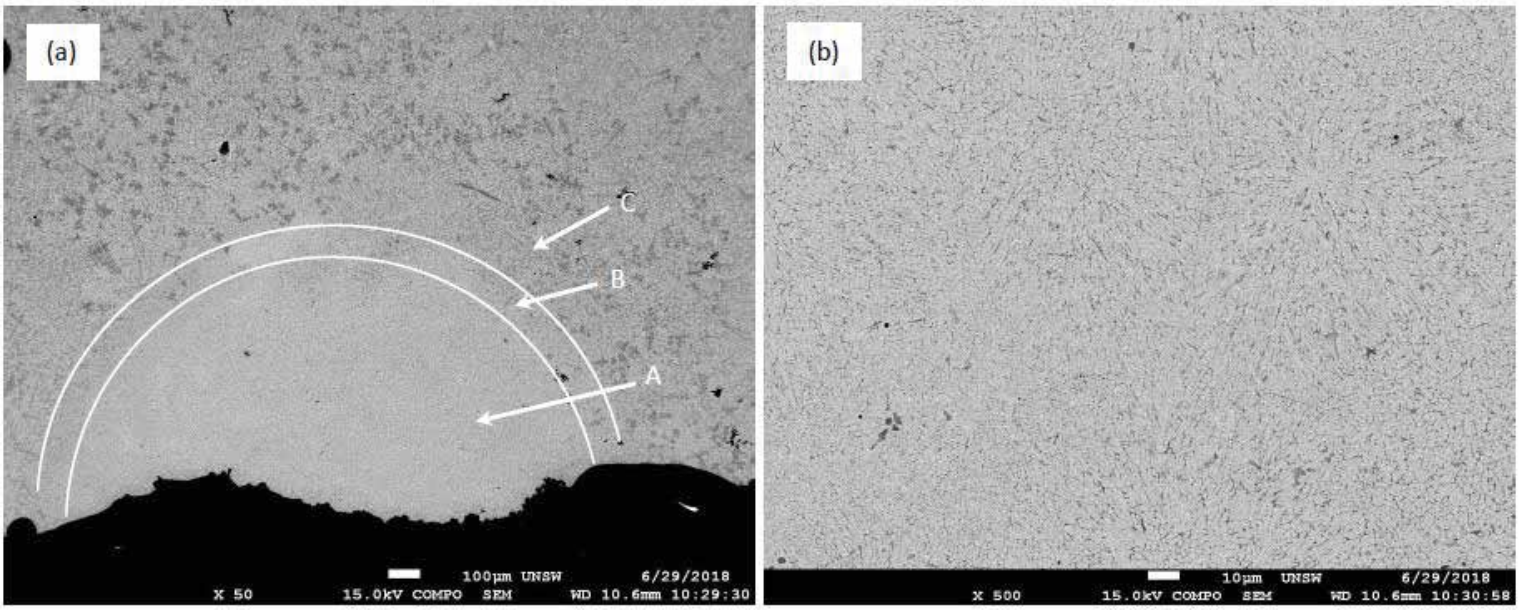

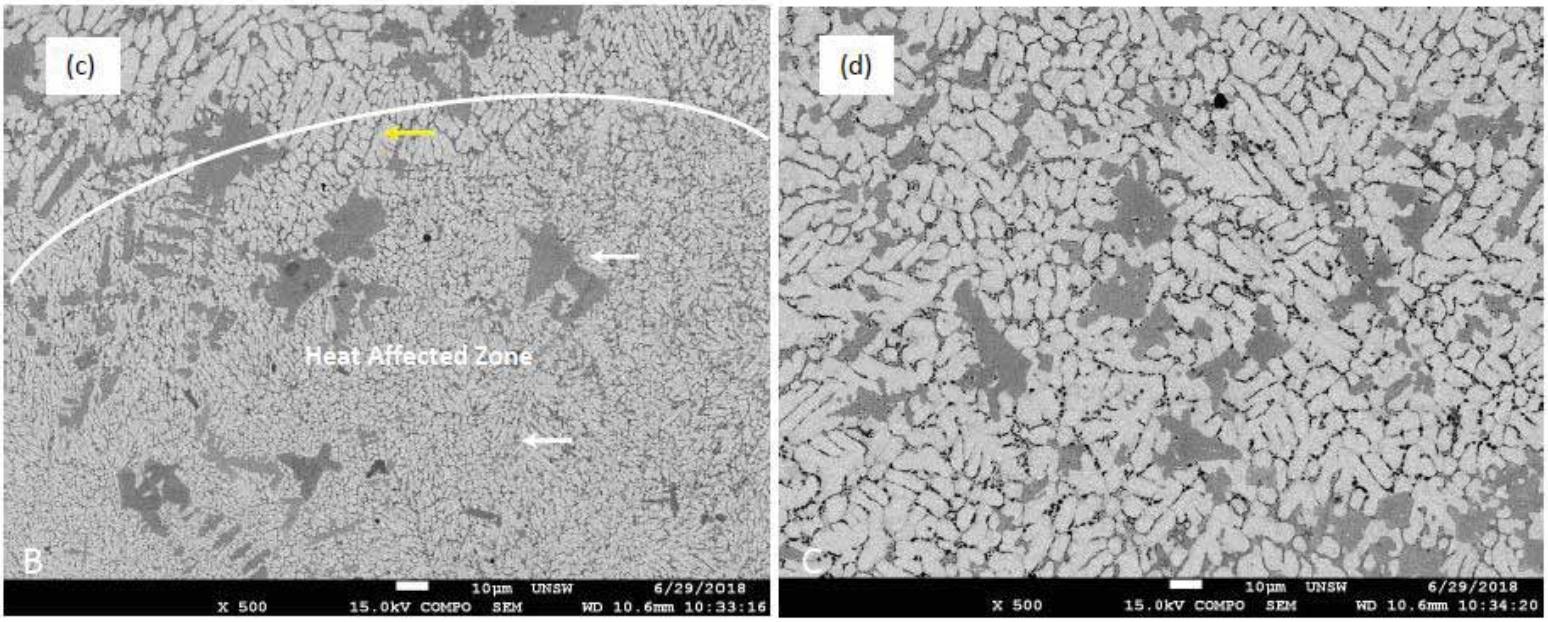

Figure 7 (a) – (d): $Zr_{47.5}Cu_{45.5}Al_5Co_2$ (0.5% inoculant) Track 1: Power 500 W, Spot size 0.61 mm, Scan speed 600 mm / min.

$Zr_{47.5}Cu_{45.5}Al_5Co_2$ (inoculant = 0.5%) Track 2

Microstructure evolved under the action of decreased power of laser (300 W) with same spot and scan speed was shown in Figures 8 (a) – (e). These were characterised by presence and appearance of typical CuZr B2 phase (spheroidal or near spheroidal), Al_2Zr fcc phase (sharp needle like / flower tip like dark grey areas) [112] and small porosity. Under the action of reduced laser power which generated less heat, size, shape and morphological features of melt pool were altered and were entirely different. Size of melt pool was decreased, it was manifested by lesser amount of turbulence, hence less spatter, denudation zones and rough corners / edges. There was small evidence of surface depression which indicated shrinkage and small internal porosity. Overall, size / span of melt pool was reduced to 850 – 900 µm at the surface while its depth was also reduced to around 550 µm. An image of melt pool at high magnification (x500) was shown in Figure 8 (b). It clearly indicated formation of monolithic 100% glassy structure with no sign or evidence of precipitation. However, as point of observation was moved further deep into sample, an area depicted by partial melting and recrystallisation was observed. This was heat affected zone (Figure 8 (c)). It clearly showed sign of fusion at certain places and then recrystallisation while some areas specially elongated Al_2Zr fcc phase were left as such. It appeared that CuZr B2 phase was melted completely while Al_2Zr fcc phase experienced partial or incomplete melting. Size of heat affected zone was very large spanning to a depth of around 220 – 230 µm. This was shown in two parts in figures 8 (c) – (d). Base metal with unaltered structure was observed in figure 8 (e). This was marked again with three structures shown and described previously.

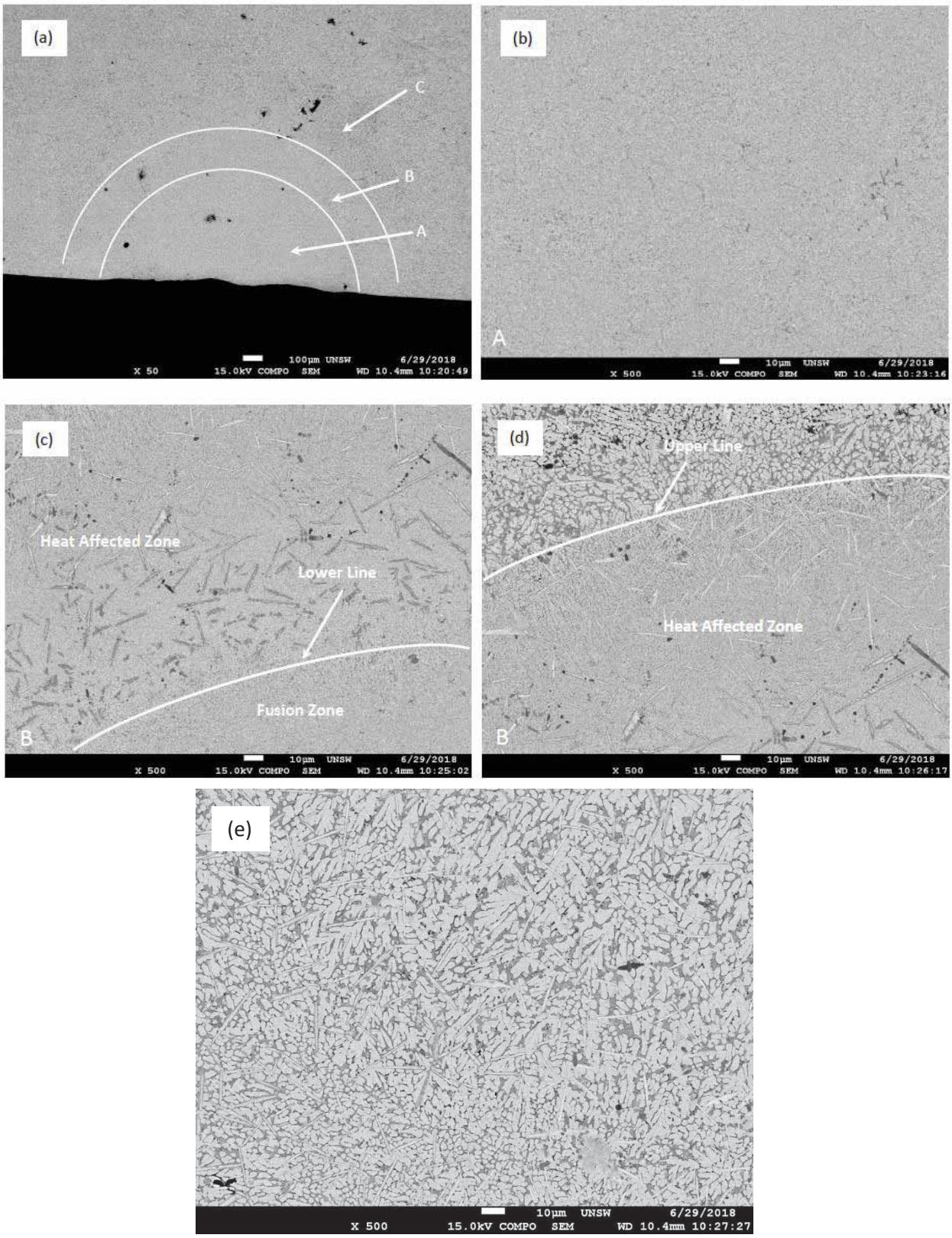

Figure 8 (a) – (e): $Zr_{47.5}Cu_{45.5}Al_5Co_2$ (0.5% inoculant) Track 2: Power 300 W, Spot size 0.61 mm, Scan speed 600 mm / min

$Zr_{47.5}Cu_{45.5}Al_5Co_2$ (inoculant = 0.5%) Track 3

Finally, when the scan speed of laser was increased to 1500 mm / minute while keeping laser power at 300 W and spot size at 0.61 mm. Melt pool, heat affected zone (HAZ) and microstructures evolved in these were shown in figures 9 (a) – (d). Surface of material experienced intense effect of heat and there were clear and marked signs of surface roughness, spatter and discontinuities. However, as the laser traversed its path quickly, size of melt pool (both in terms of width and depth) was not very large. It spaned at around 70 µm on the surface while its depth was almost similar. There was no indication of precipitation or recrystallization of any phase in melt pool and at higher magnification (x500) (Figure 9 (b)). Melt pool depicted placid glassy structure with no crystals. There was however, slight effect of burning at the surface which was characteristic of intense heat. Size of heat affected zone (HAZ) beneath fusion zone was not profound as well. It merely had a depth of around 120 µm. Features observed in this were fused and rapidly solidified glass and small brittle Al_2Zr fcc phase. Al_2Zr fcc phase showed tint of silvery or light grey areas typical of this phase as observed previously as well. Surprisingly, there was no observation of spherulites in fusion zone or HAZ of any of inoculated samples (0.25% as well as 0.5%) and it may be inferred that inoculation resisted change of morphology. Structure was found in unaltered state in base metal and found to have small to medium size precipitates around 4 – 6 µm in size. Overall effect of intense heat from localised source of energy was found to cast change in microstructure.

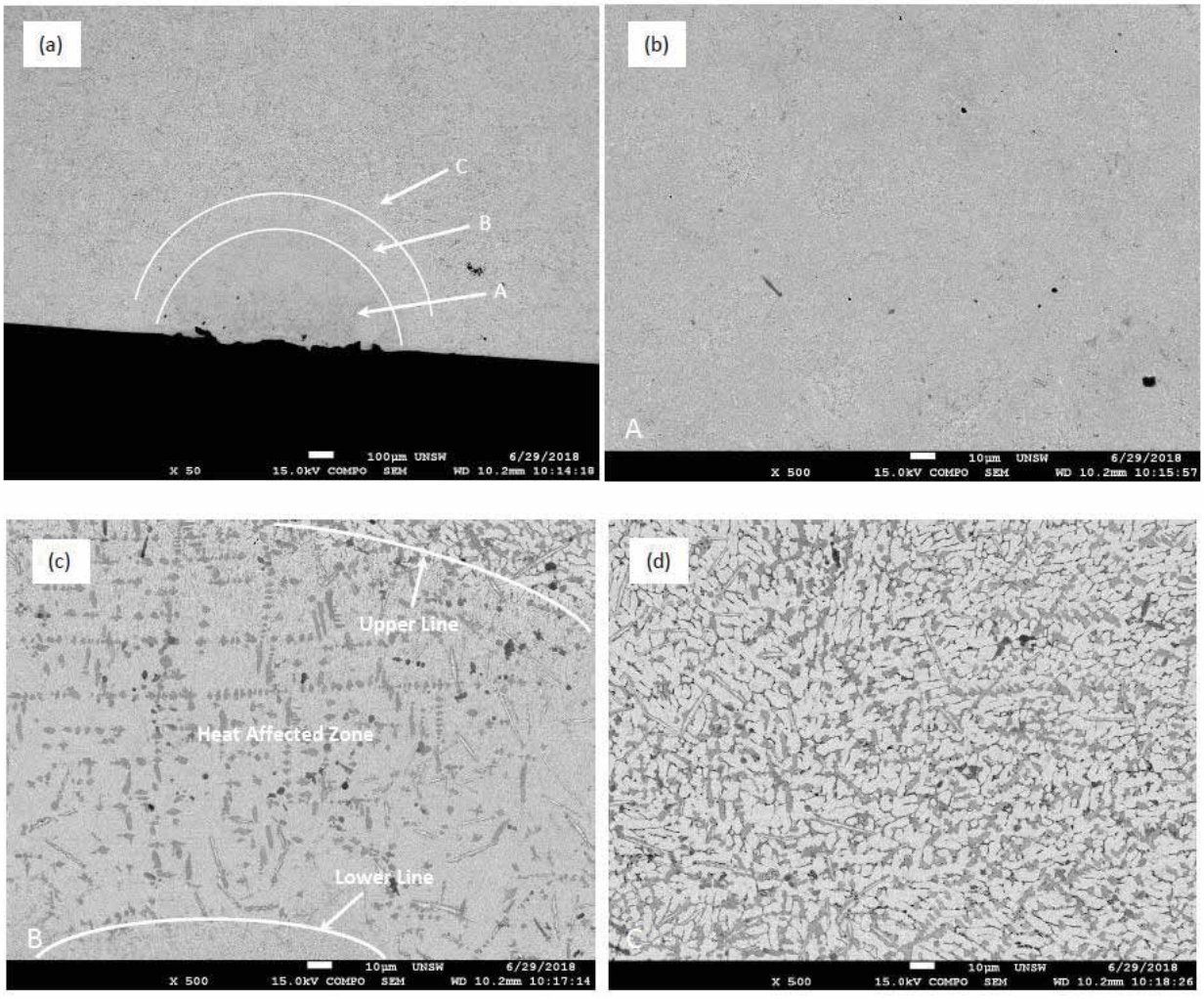

Figure 9 (a) – (d): $Zr_{47.5}Cu_{45.5}Al_5Co_2$ (0.5% inoculant) Track 3: Power 300 W, spot size 0.61 mm, Scan speed 1500 mm / min.

Conclusions

In general, following conclusions could be drawn

a. Inoculation treatment casted an effect of refinement on microstructure (grain size, its count and distribution).
b. ZrC was found to be an effective new inoculant for bulk metallic glass matrix composites.
c. As the percentage of inoculant increased from zero to 0.5%, type, size, shape and morphology of phases changed, and their amount increased.
d. The CuZr B2 phase becomes refined and decreases from around 4 μm to 2.8 μm with increase of percentage of inoculant from zero to 0.25% while increased slightly when percentage of inoculant increased to 0.5% indicating non-linearity.
e. Another phase namely brittle Al_2Zr fcc phase (small to medium columnar dendrites) was also observed to form out of glassy melt.
f. Morphology of CuZr B2 changed from spheroids to spherulite under the effect of intense heat observed only when laser power was 500 W and there was no inoculation.
g. Inoculation was found to resist change of morphology of phases in melted and rapidly solidified material as no evidence of spherulites was observed in samples treated with ZrC.

Acknowledgements

Authors would like to thank Dr. Daniel East (CSIRO) for providing experimental facilities for melting and casting of samples, Dr. Dong Qiu (also author) for design of inoculants and providing their samples, Mr. Alan Jones (Additive Manufacturing Precinct, RMIT University) for performing laser surface treatment, Mr. Jeremy Gonzalez (Massachusetts Materials Research Inc., Worcester, MA) for cutting, mounting, grinding and polishing of samples and Dr. Simon Hager (The University of New South Wales, Sydney) for help in performing scanning electron microscopy in back scatter electron imaging mode. Lead author would also like to thank Prof. Milan Brandt (also author) for moral support, patience, helpful scientific discussion and guidance and RMIT University for providing stipend for tuition and living.

References

1. Avner, S.H., *Introduction to physical metallurgy*. 1974: McGraw-Hill.
2. Porter, D.A. and K.E. Easterling, *Phase Transformations in Metals and Alloys, Third Edition (Revised Reprint)*. 1992: Taylor & Francis.
3. Taylor, H.F., *Foundry engineering*. 1959: Wiley.
4. Kurz, W. and D.J. Fisher, *Fundamentals of solidification*. 1986: Trans Tech Publications.
5. Klement, W., R.H. Willens, and P.O.L. Duwez, *Non-crystalline Structure in Solidified Gold-Silicon Alloys.* Nature, 1960. **187**(4740): p. 869-870.
6. Telford, M., *The case for bulk metallic glass.* Materials Today, 2004. **7**(3): p. 36-43.
7. Chen, M., *A brief overview of bulk metallic glasses.* NPG Asia Mater, 2011. **3**: p. 82-90.
8. Schroers, J. and W.L. Johnson, *Ductile Bulk Metallic Glass.* Physical Review Letters, 2004. **93**(25): p. 255506.

9. Greer, A.L., *Metallic Glasses.* Science, 1995. **267**(5206): p. 1947-1953.
10. Güntherodt, H.J., *Metallic glasses*, in *Festkörperprobleme 17: Plenary Lectures of the Divisions "Semiconductor Physics" "Metal Physics" "Low Temperature Physics" "Thermodynamics and Statistical Physics" "Crystallography" "Magnetism" "Surface Physics" of the German Physical Society Münster, March 7–12, 1977*, J. Treusch, Editor. 1977, Springer Berlin Heidelberg: Berlin, Heidelberg. p. 25-53.
11. Ashby, M.F. and A.L. Greer, *Metallic glasses as structural materials.* Scripta Materialia, 2006. **54**(3): p. 321-326.
12. Si, J.J., et al., *Cr-based bulk metallic glasses with ultrahigh hardness.* Applied Physics Letters, 2015. **106**(25): p. 251905.
13. Ramamurty, U., et al., *Hardness and plastic deformation in a bulk metallic glass.* Acta Materialia, 2005. **53**(3): p. 705-717.
14. Greer, A.L., Y.Q. Cheng, and E. Ma, *Shear bands in metallic glasses.* Materials Science and Engineering: R: Reports, 2013. **74**(4): p. 71-132.
15. Yang, Y. and C.T. Liu, *Size effect on stability of shear-band propagation in bulk metallic glasses: an overview.* Journal of materials science, 2012. **47**(1): p. 55-67.
16. Packard, C.E. and C.A. Schuh, *Initiation of shear bands near a stress concentration in metallic glass.* Acta Materialia, 2007. **55**(16): p. 5348-5358.
17. Zhu, Z., et al., *Ta-particulate reinforced Zr-based bulk metallic glass matrix composite with tensile plasticity.* Scripta Materialia, 2010. **62**(5): p. 278-281.
18. Fan, C., et al., *Mechanical Behavior of Bulk Amorphous Alloys Reinforced by Ductile Particles at Cryogenic Temperatures.* Physical Review Letters, 2006. **96**(14): p. 145506.
19. Choi-Yim, H., et al., *Processing, microstructure and properties of ductile metal particulate reinforced Zr57Nb5Al10Cu15.4Ni12.6 bulk metallic glass composites.* Acta Materialia, 2002. **50**(10): p. 2737-2745.
20. Liu, J., et al., *In situ spherical B2 CuZr phase reinforced ZrCuNiAlNb bulk metallic glass matrix composite.* Journal of Materials Research, 2010. **25**(6): p. 1159-1163.
21. Fan, C., R.T. Ott, and T.C. Hufnagel, *Metallic glass matrix composite with precipitated ductile reinforcement.* Applied Physics Letters, 2002. **81**(6): p. 1020-1022.
22. Jiang, F., et al., *Microstructure evolution and mechanical properties of Cu46Zr47Al7 bulk metallic glass composite containing CuZr crystallizing phases.* Materials Science and Engineering: A, 2007. **467**(1–2): p. 139-145.
23. Chen, G., et al., *Enhanced plasticity in a Zr-based bulk metallic glass composite with in situ formed intermetallic phases.* Applied Physics Letters, 2009. **95**(8): p. 081908.
24. Guo, W. and H. Kato, *Development and microstructure optimization of Mg-based metallic glass matrix composites with in situ B2-NiTi dispersoids.* Materials & Design, 2015. **83**: p. 238-248.
25. Jeon, C., et al., *Effects of Effective Dendrite Size on Tensile Deformation Behavior in Ti-Based Dendrite-Containing Amorphous Matrix Composites Modified from Ti-6Al-4V Alloy.* Metallurgical and Materials Transactions A, 2015. **46**(1): p. 235-250.
26. Zhang, T., et al., *Dendrite size dependence of tensile plasticity of in situ Ti-based metallic glass matrix composites.* Journal of Alloys and Compounds, 2014. **583**: p. 593-597.
27. Hofmann, D.C., et al., *Castable Bulk Metallic Glass Strain Wave Gears: Towards Decreasing the Cost of High-Performance Robotics.* Scientific Reports, 2016. **6**: p. 37773.
28. Rafique, M.M.A., *Production and Characterization of Zr Based Bulk Metallic Glass Matrix Composites (BMGMC) in the Form of Wedge Shape Ingots.* Engineering, 2018. **Vol.10No.04**: p. 31.
29. Kim, D.H., et al., *Phase separation in metallic glasses.* Progress in Materials Science, 2013. **58**(8): p. 1103-1172.

30. Basu, J., et al., *Microstructure and mechanical properties of a partially crystallized La-based bulk metallic glass.* Philosophical Magazine, 2003. **83**(15): p. 1747-1760.
31. Taub, A.I. and F. Spaepen, *The kinetics of structural relaxation of a metallic glass.* Acta Metallurgica, 1980. **28**(12): p. 1781-1788.
32. Zhang, Y., W.H. Wang, and A.L. Greer, *Making metallic glasses plastic by control of residual stress.* Nature Materials, 2006. **5**: p. 857.
33. Fan, C., et al., *Properties of as-cast and structurally relaxed Zr-based bulk metallic glasses.* Journal of Non-Crystalline Solids, 2006. **352**(2): p. 174-179.
34. Krämer, L., Y. Champion, and R. Pippan, *From powders to bulk metallic glass composites.* Scientific Reports, 2017. **7**(1): p. 6651.
35. Brothers, A.H. and D.C. Dunand, *Ductile Bulk Metallic Glass Foams.* Advanced Materials, 2005. **17**(4): p. 484-486.
36. Liu, Z., et al., *Pronounced ductility in CuZrAl ternary bulk metallic glass composites with optimized microstructure through melt adjustment.* AIP Advances, 2012. **2**(3): p. 032176.
37. Cheng, J.-L., et al., *Innovative approach to the design of low-cost Zr-based BMG composites with good glass formation.* Scientific Reports, 2013. **3**: p. 2097.
38. Harooni, A., et al., *Processing window development for laser cladding of zirconium on zirconium alloy.* Journal of Materials Processing Technology, 2016. **230**: p. 263-271.
39. Hays, C.C., C.P. Kim, and W.L. Johnson, *Microstructure Controlled Shear Band Pattern Formation and Enhanced Plasticity of Bulk Metallic Glasses Containing \textit{in situ} Formed Ductile Phase Dendrite Dispersions.* Physical Review Letters, 2000. **84**(13): p. 2901-2904.
40. Scudino, S., et al., *Ductile bulk metallic glasses produced through designed heterogeneities.* Scripta Materialia, 2011. **65**(9): p. 815-818.
41. Gargarella, P., et al., *Phase formation and mechanical properties of Ti–Cu–Ni–Zr bulk metallic glass composites.* Acta Materialia, 2014. **65**: p. 259-269.
42. Das, J., et al., *``Work-Hardenable'' Ductile Bulk Metallic Glass.* Physical Review Letters, 2005. **94**(20): p. 205501.
43. Das, J., et al., *Plasticity in bulk metallic glasses investigated via the strain distribution.* Physical Review B, 2007. **76**(9): p. 092203.
44. Kim, K.B., et al., *Heterogeneous distribution of shear strains in deformed Ti66.1Cu8Ni4.8Sn7.2Nb13.9 nanostructure-dendrite composite.* physica status solidi (a), 2005. **202**(13): p. 2405-2412.
45. Fan, C., C. Li, and A. Inoue, *Nanocrystal composites in Zr–Nb–Cu–Al metallic glasses.* Journal of Non-Crystalline Solids, 2000. **270**(1–3): p. 28-33.
46. Inoue, A., et al., *Production methods and properties of engineering glassy alloys and composites.* Intermetallics, 2015. **58**: p. 20-30.
47. Hofmann, D.C., et al., *Designing metallic glass matrix composites with high toughness and tensile ductility.* Nature, 2008. **451**: p. 1085.
48. Hofmann, D.C., et al., *Development of tough, low-density titanium-based bulk metallic glass matrix composites with tensile ductility.* Proceedings of the National Academy of Sciences, 2008. **105**(51): p. 20136-20140.
49. Zhang, L., et al., *Distribution of Be in a Ti-Based Bulk Metallic Glass Composite Containing B-Ti.* Journal of Materials Science & Technology, 2017. **33**(7): p. 708-711.
50. Booth, J., J. Lewandowski, and J. Carter, *EBSD Analysis for Microstructure Characterization of Zr-based Bulk Metallic Glass Composites.* Microscopy and Microanalysis, 2014. **20**(S3): p. 852-853.
51. Hofmann, D.C. and W.L. Johnson. *Improving Ductility in Nanostructured Materials and Metallic Glasses:"Three Laws"*. in *Materials Science Forum*. 2010. Trans Tech Publ.

52. Jiang, J.-Z., et al., *Low-Density High-Strength Bulk Metallic Glasses and Their Composites: A Review.* Advanced Engineering Materials, 2015. **17**(6): p. 761-780.
53. Qiao, J., H. Jia, and P.K. Liaw, *Metallic glass matrix composites.* Materials Science and Engineering: R: Reports, 2016. **100**: p. 1-69.
54. Sun, H. and K.M. Flores, *Microstructural Analysis of a Laser-Processed Zr-Based Bulk Metallic Glass.* Metallurgical and Materials Transactions A, 2010. **41**(7): p. 1752-1757.
55. Rafique, M.M.A., *Modelling and Simulation of Solidification Phenomena during Additive Manufacturing of Bulk Metallic Glass Matrix Composites (BMGMC)¡ªA Brief Review and Introduction of Technique.* Journal of Encapsulation and Adsorption Sciences, 2018. **Vol.08No.02**: p. 50.
56. Park, E.S. and D.H. Kim, *Design of Bulk metallic glasses with high glass forming ability and enhancement of plasticity in metallic glass matrix composites: A review.* Metals and Materials International, 2005. **11**(1): p. 19-27.
57. Gibson, I., W.D. Rosen, and B. Stucker, *Development of Additive Manufacturing Technology*, in *Additive Manufacturing Technologies: Rapid Prototyping to Direct Digital Manufacturing*. 2010, Springer US: Boston, MA. p. 36-58.
58. Frazier, W.E., *Metal Additive Manufacturing: A Review.* Journal of Materials Engineering and Performance, 2014. **23**(6): p. 1917-1928.
59. Sames, W.J., et al., *The metallurgy and processing science of metal additive manufacturing.* International Materials Reviews, 2016. **61**(5): p. 315-360.
60. Wong, K.V. and A. Hernandez, *A Review of Additive Manufacturing.* ISRN Mechanical Engineering, 2012. **2012**: p. 10.
61. DebRoy, T., et al., *Additive manufacturing of metallic components – Process, structure and properties.* Progress in Materials Science, 2018. **92**: p. 112-224.
62. Yap, C.Y., et al., *Review of selective laser melting: Materials and applications.* Applied Physics Reviews, 2015. **2**(4): p. 041101.
63. Zheng, B., et al., *Thermal Behavior and Microstructural Evolution during Laser Deposition with Laser-Engineered Net Shaping: Part I. Numerical Calculations.* Metallurgical and Materials Transactions A, 2008. **39**(9): p. 2228-2236.
64. Romano, J., et al., *Temperature distribution and melt geometry in laser and electron-beam melting processes – A comparison among common materials.* Additive Manufacturing, 2015. **8**: p. 1-11.
65. Gong, X. and K. Chou, *Phase-Field Modeling of Microstructure Evolution in Electron Beam Additive Manufacturing.* JOM, 2015. **67**(5): p. 1176-1182.
66. Zhang, Y., et al., *Microstructural analysis of Zr55Cu30Al10Ni5 bulk metallic glasses by laser surface remelting and laser solid forming.* Intermetallics, 2015. **66**: p. 22-30.
67. Olakanmi, E.O., R.F. Cochrane, and K.W. Dalgarno, *A review on selective laser sintering/melting (SLS/SLM) of aluminium alloy powders: Processing, microstructure, and properties.* Progress in Materials Science, 2015. **74**: p. 401-477.
68. Li, X.P., et al., *Selective laser melting of Zr-based bulk metallic glasses: Processing, microstructure and mechanical properties.* Materials & Design, 2016. **112**: p. 217-226.
69. Yang, G., et al., *Laser solid forming Zr-based bulk metallic glass.* Intermetallics, 2012. **22**: p. 110-115.
70. Welk, B.A., et al., *Phase Selection in a Laser Surface Melted Zr-Cu-Ni-Al-Nb Alloy.* Metallurgical and Materials Transactions B, 2014. **45**(2): p. 547-554.
71. Cardinal, S., et al., *Manufacturing of Cu-based metallic glasses matrix composites by spark plasma sintering.* Materials Science and Engineering: A, 2018. **711**: p. 405-414.
72. Buchbinder, D., et al., *High Power Selective Laser Melting (HP SLM) of Aluminum Parts.* Physics Procedia, 2011. **12**: p. 271-278.

73. Zheng, B., et al., *Processing and Behavior of Fe-Based Metallic Glass Components via Laser-Engineered Net Shaping.* Metallurgical and Materials Transactions A, 2009. **40**(5): p. 1235-1245.
74. Dezfoli, A.R.A., et al., *Determination and controlling of grain structure of metals after laser incidence: Theoretical approach.* Scientific Reports, 2017. **7**: p. 41527.
75. Zinoviev, A., et al., *Evolution of grain structure during laser additive manufacturing. Simulation by a cellular automata method.* Materials & Design, 2016. **106**: p. 321-329.
76. Khairallah, S.A., et al., *Laser powder-bed fusion additive manufacturing: Physics of complex melt flow and formation mechanisms of pores, spatter, and denudation zones.* Acta Materialia, 2016. **108**: p. 36-45.
77. Zhang, J., et al. *Probabilistic simulation of solidification microstructure evolution during laser-based metal deposition*. in *Proceedings of 2013 Annual International Solid Freeform Fabrication Symposium–An Additive Manufacturing Conference*. 2013.
78. Lindgren, L.-E., et al., *Simulation of additive manufacturing using coupled constitutive and microstructure models.* Additive Manufacturing.
79. Musaddique Ali Rafique, M., *Simulation of Solidification Parameters during Zr Based Bulk Metallic Glass Matrix Composite's (BMGMCs) Additive Manufacturing*. Vol. 10. 2018. 85-108.
80. Rafique, M.M.A., D. Qiu, and M. Easton, *Modeling and simulation of microstructural evolution in Zr based Bulk Metallic Glass Matrix Composites during solidification.* MRS Advances. **2**(58-59): p. 3591-3606.
81. Li, Y. and D. Gu, *Thermal behavior during selective laser melting of commercially pure titanium powder: Numerical simulation and experimental study.* Additive Manufacturing, 2014. **1–4**: p. 99-109.
82. Baufeld, B., E. Brandl, and O. van der Biest, *Wire based additive layer manufacturing: Comparison of microstructure and mechanical properties of Ti–6Al–4V components fabricated by laser-beam deposition and shaped metal deposition.* Journal of Materials Processing Technology, 2011. **211**(6): p. 1146-1158.
83. Li, B., et al., *Laser welding of Zr45Cu48Al7 bulk glassy alloy.* Journal of Alloys and Compounds, 2006. **413**(1–2): p. 118-121.
84. Pauly, S., et al., *Processing metallic glasses by selective laser melting.* Materials Today, 2013. **16**(1–2): p. 37-41.
85. Kim, J.H., et al., *Pulsed Nd:YAG laser welding of Cu54Ni6Zr22Ti18 bulk metallic glass.* Materials Science and Engineering: A, 2007. **449–451**: p. 872-875.
86. Matthews, D.T.A., V. Ocelík, and J.T.M. de Hosson, *Tribological and mechanical properties of high power laser surface-treated metallic glasses.* Materials Science and Engineering: A, 2007. **471**(1): p. 155-164.
87. Chen, B., et al., *Improvement in mechanical properties of a Zr-based bulk metallic glass by laser surface treatment.* Journal of Alloys and Compounds, 2010. **504**: p. S45-S47.
88. Wu, G., et al., *Induced multiple heterogeneities and related plastic improvement by laser surface treatment in CuZr-based bulk metallic glass.* Intermetallics, 2012. **24**: p. 50-55.
89. Williams, E. and N. Lavery, *Laser processing of bulk metallic glass: A review.* Journal of Materials Processing Technology, 2017. **247**: p. 73-91.
90. Ouyang, D., N. Li, and L. Liu, *Structural heterogeneity in 3D printed Zr-based bulk metallic glass by selective laser melting.* Journal of Alloys and Compounds, 2018. **740**: p. 603-609.
91. Zhang, C., et al., *3D printing of Fe-based bulk metallic glasses and composites with large dimension and enhanced toughness by thermal spraying*. Vol. 6. 2018.
92. Ouyang, D., et al., *3D printing of crack-free high strength Zr-based bulk metallic glass composite by selective laser melting.* Intermetallics, 2017. **90**: p. 128-134.

93. Shen, Y., et al., *3D printing of large, complex metallic glass structures.* Materials & Design, 2017. **117**: p. 213-222.
94. Gibson, M.A., et al., *3D printing metals like thermoplastics: Fused filament fabrication of metallic glasses.* Materials Today, 2018.
95. Matthews, D.T.A., et al., *Laser engineered surfaces from glass forming alloy powder precursors: Microstructure and wear.* Surface and Coatings Technology, 2009. **203**(13): p. 1833-1843.
96. Wang, H.-S., et al., *The effects of initial welding temperature and welding parameters on the crystallization behaviors of laser spot welded Zr-based bulk metallic glass.* Materials Chemistry and Physics, 2011. **129**(1): p. 547-552.
97. Wang, H.-S., J.-Y. Wu, and Y.-T. Liu, *Effect of the volume fraction of the ex-situ reinforced Ta additions on the microstructure and properties of laser-welded Zr-based bulk metallic glass composites.* Intermetallics, 2016. **68**: p. 87-94.
98. Wang, H.S., et al., *Combination of a Nd:YAG laser and a liquid cooling device to (Zr53Cu30Ni9Al8)Si0.5 bulk metallic glass welding.* Materials Science and Engineering: A, 2010. **528**(1): p. 338-341.
99. Zhu, Y., et al., *Effect of nanosecond pulse laser ablation on the surface morphology of Zr-based metallic glass.* Optics & Laser Technology, 2016. **83**: p. 21-27.
100. Williams, E. and E.B. Brousseau, *Nanosecond laser processing of Zr41.2Ti13.8Cu12.5Ni10Be22.5 with single pulses.* Journal of Materials Processing Technology, 2016. **232**: p. 34-42.
101. Fu, J., et al., *Effect of laser shock peening on the compressive deformation and plastic behavior of Zr-based bulk metallic glass.* Optics and Lasers in Engineering, 2016. **86**: p. 53-61.
102. Audebert, F., et al., *Production of glassy metallic layers by laser surface treatment.* Scripta Materialia, 2003. **48**(3): p. 281-286.
103. Ma, F., et al., *Femtosecond laser-induced concentric ring microstructures on Zr-based metallic glass.* Applied Surface Science, 2010. **256**(11): p. 3653-3660.
104. Heine, R.W., C.R. Loper, and P.C. Rosenthal, *Principles of Metal Casting*. 1955: McGraw-Hill.
105. Chalmers, B., *Principles of Solidification*, in *Applied Solid State Physics*, W. Low and M. Schieber, Editors. 1970, Springer US: Boston, MA. p. 161-170.
106. Xu, W., et al., *In situ formation of crystalline flakes in Mg-based metallic glass composites by controlled inoculation*. Vol. 59. 2011. 7776-7786.
107. Stefanescu, D., *Science and engineering of casting solidification*. 2015: Springer.
108. Flemings, M.C., *Solidification Processing*. 1974: McGraw-Hill.
109. Christian, J.W., *The Theory of Transformations in Metals and Alloys*. 2002: Elsevier Science.
110. Yue, T.M., Y.P. Su, and H.O. Yang, *Laser cladding of Zr65Al7.5Ni10Cu17.5 amorphous alloy on magnesium.* Materials Letters, 2007. **61**(1): p. 209-212.
111. Wang, Y., et al., *Microstructure and properties of laser clad Zr-based alloy coatings on Ti substrates.* Surface and Coatings Technology, 2004. **176**(3): p. 284-289.
112. Jiang, S.-S., et al., *A CuZr-based bulk metallic glass composite with excellent mechanical properties by optimizing microstructure.* Journal of Non-Crystalline Solids, 2018. **483**: p. 94-98.
113. Rafique, M.M.A., *Effect of Inoculation on Phase Formation and Indentation Hardness Behaviour of Zr_{47.5}Cu_{45.5}Al₅Co ₂ and Zr₆₅Cu₁₅Al₁₀Ni< SUB>10</SUB> Bulk Metallic Glass Matrix Composites.* Engineering, 2018. **Vol.10No.08**: p. 30.